ELECTRONIC SUPPORTING INFORMATION

((R)-(−)-3-hydroxyquinuclidium)[$FeCl_4$]; A Plastic Hybrid Compound with Chirality, Multiaxial Ferroelectricity and Long Range Magnetic Ordering

Palmerina González-Izquierdo,*[a,b] Oscar Fabelo,*[b] Laura Cañadillas-Delgado,[b] Garikoitz Beobide,[c,d] Oriol Vallcorba,[e] Jorge Salgado-Beceiro,[f] Manuel Sánchez-Andújar,[f] Carmen Martin,[g] Javier Ruiz-Fuentes,[a] José Eduardo García[h] María Teresa Fernández-Díaz[b] and Imanol de Pedro*[a]

[a] CITIMAC, Facultad de Ciencias, Universidad de Cantabria, 39005 Santander.
[b] Institut Laue-Langevin, BP 156X, F-38042 Grenoble Cedex, France.
[c] Departamento de Química Inorgánica, Facultad de Ciencia y Tecnología, Universidad del País Vasco, Apartado 644, E-48080, Bilbao, Spain.
[d] Basque Ctr Mat Applicat & Nanostruct, BCMat, UPV EHU Sci Pk, Leioa 48940, Spain.
[e] ALBA Synchrotron Light Source, Cerdanyola del Vallés, Barcelona, Spain.
[f] QuiMolMat Group, Department of Chemistry, Faculty of Science and Advanced Scientific Research Center (CICA), Zapateira, University of A Coruna, 15071 A Coruna, Spain.
[g] Departamento de Química Física, Facultad de Química, Universidad de Sevilla, c/Profesor García González s/n, 41012 Sevilla (Spain)
[h] Department of Physics, Universitat Politècnica de Catalunya—BarcelonaTech, 08034 Barcelona, Spain

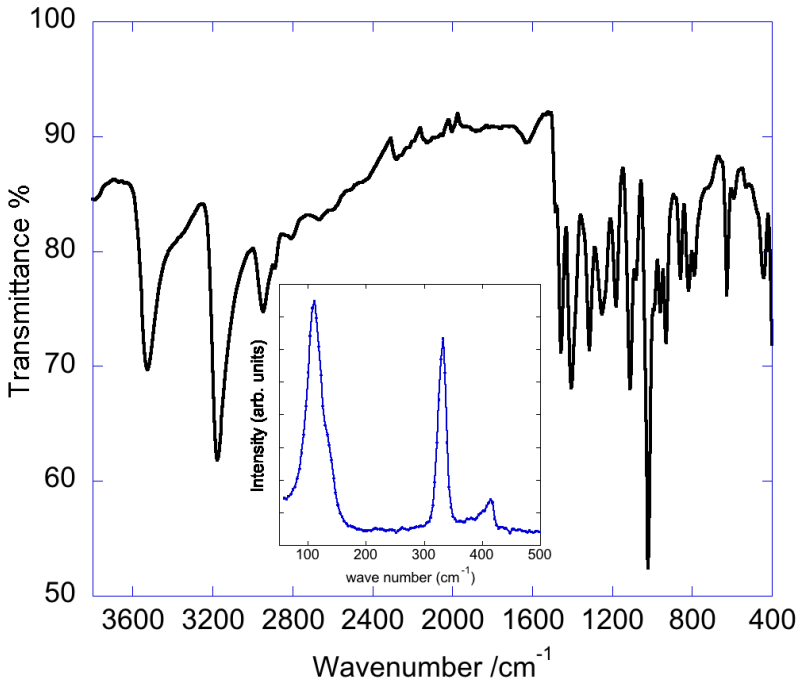

Fig. S1. IR spectra of ((R)-(−)-3-hydroxyquinuclidium)[$FeCl_4$].The inset shows the low frequency of Raman spectra.

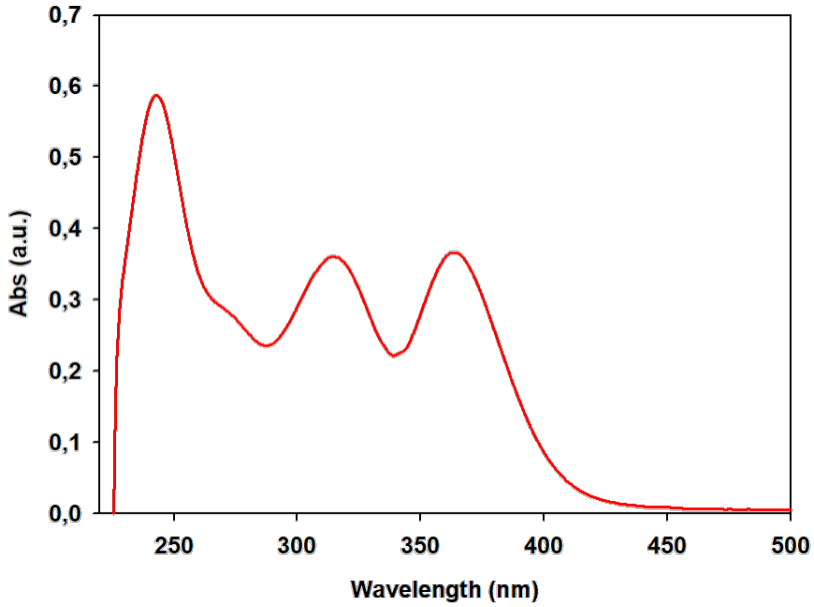

Fig. S2. UV-Vis spectrum of ((R)-(−)-3-hydroxyquinuclidium)[$FeCl_4$] in CH_2Cl_2 at 25 ºC. [FeQ] = 0.06 mM.

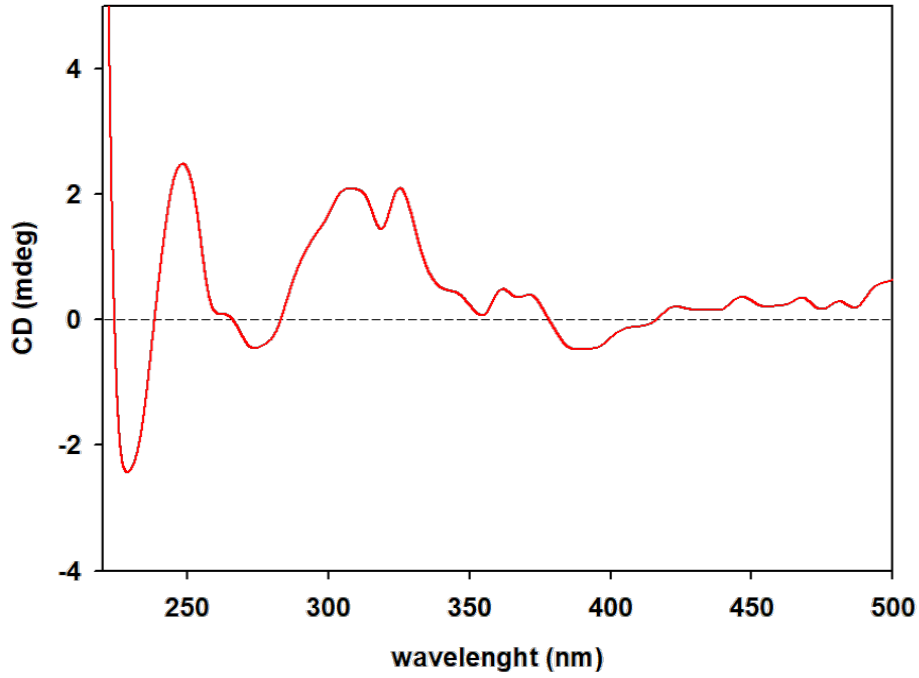

Fig. S3. CD spectrum of ((R)-(−)-3-hydroxyquinuclidium)[$FeCl_4$] in CH_2Cl_2 at 25 ºC. [FeQ] = 0.3 mM.

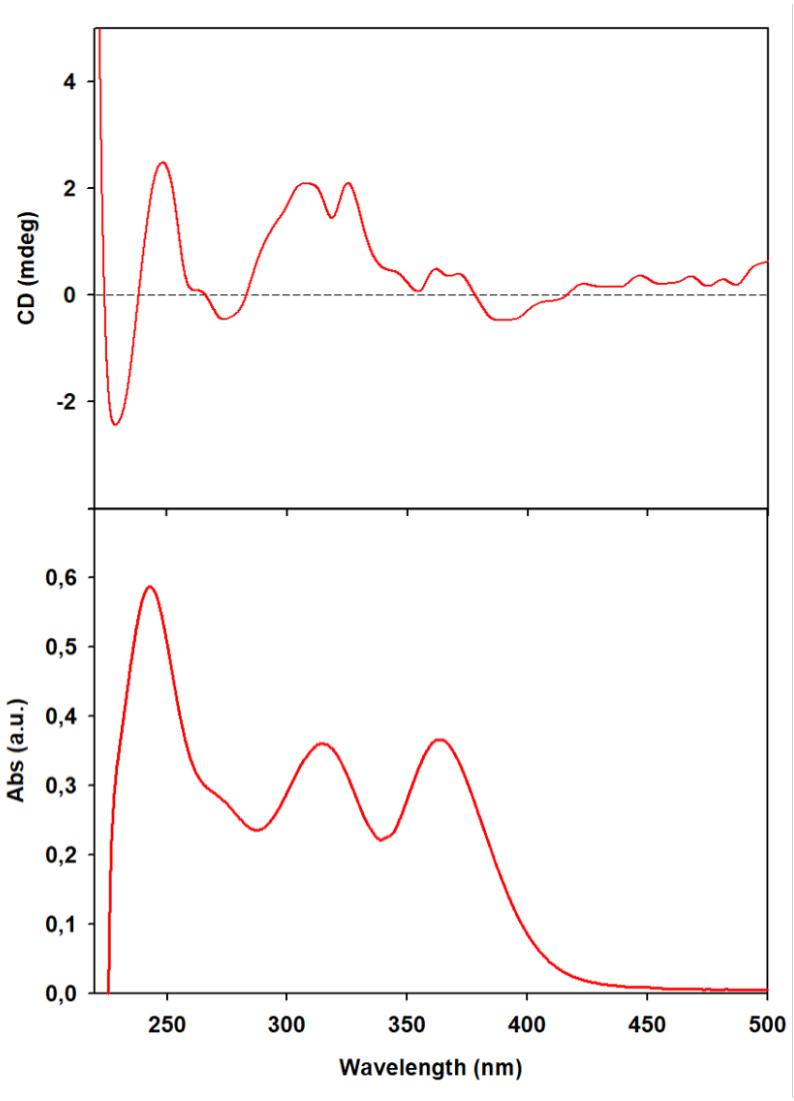

Fig. S4. CD and UV-Vis spectra of ((R)-(−)-3-hydroxyquinuclidium)[$FeCl_4$] in CH_2Cl_2 at 25 ºC.

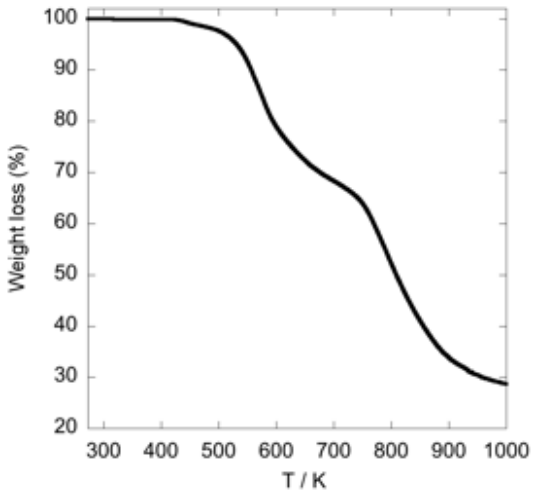

Fig.S5. TG curve recorded in inert atmosphere.

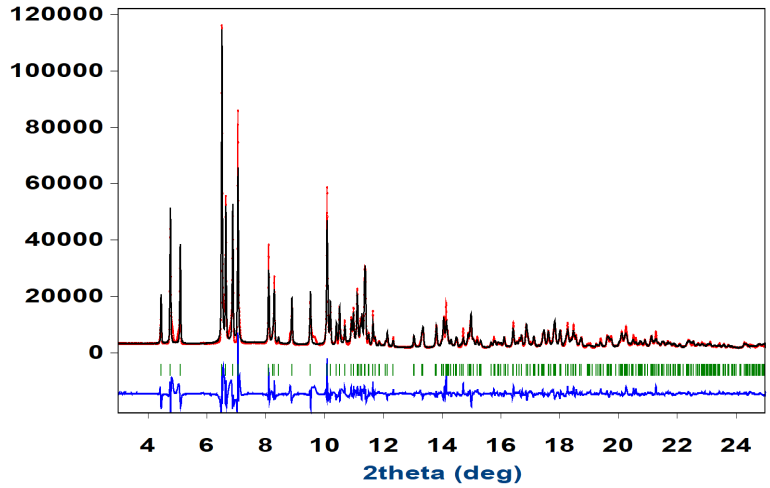

Fig.S6: Rietveld refinement to the SR-XRPD data at 100 K. Observed (red points) and calculated (black solid line) powder diffraction patterns for positions of the Bragg reflections are represented by green vertical bars. The observed-calculated difference patterns are depicted as a blue line. R_{Bragg} = 6.87.

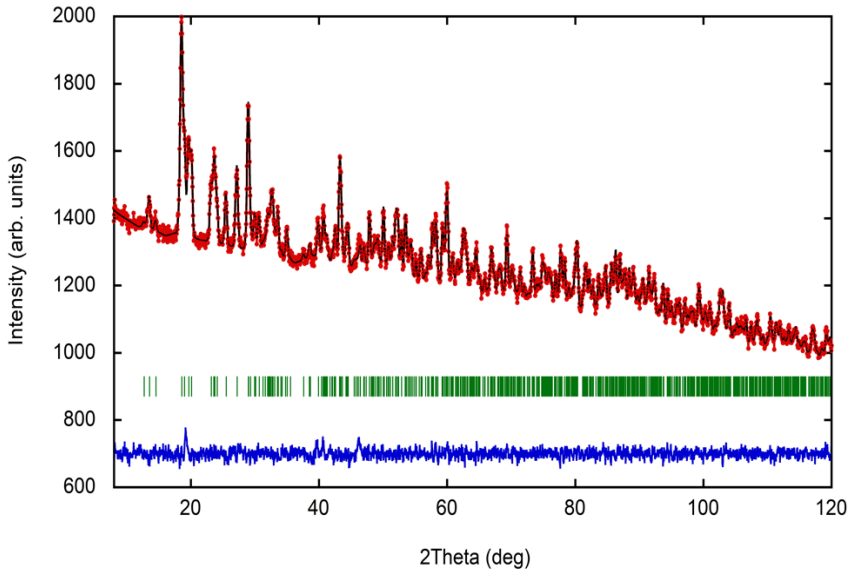

Fig. S7: Rietveld refinement to the D2B data at 10 K. Observed (red points) and calculated (black solid line) powder diffraction patterns for positions of the Bragg reflections are represented by green vertical bars. The observed-calculated difference patterns are depicted as a blue line. R_{Bragg} = 3.84.

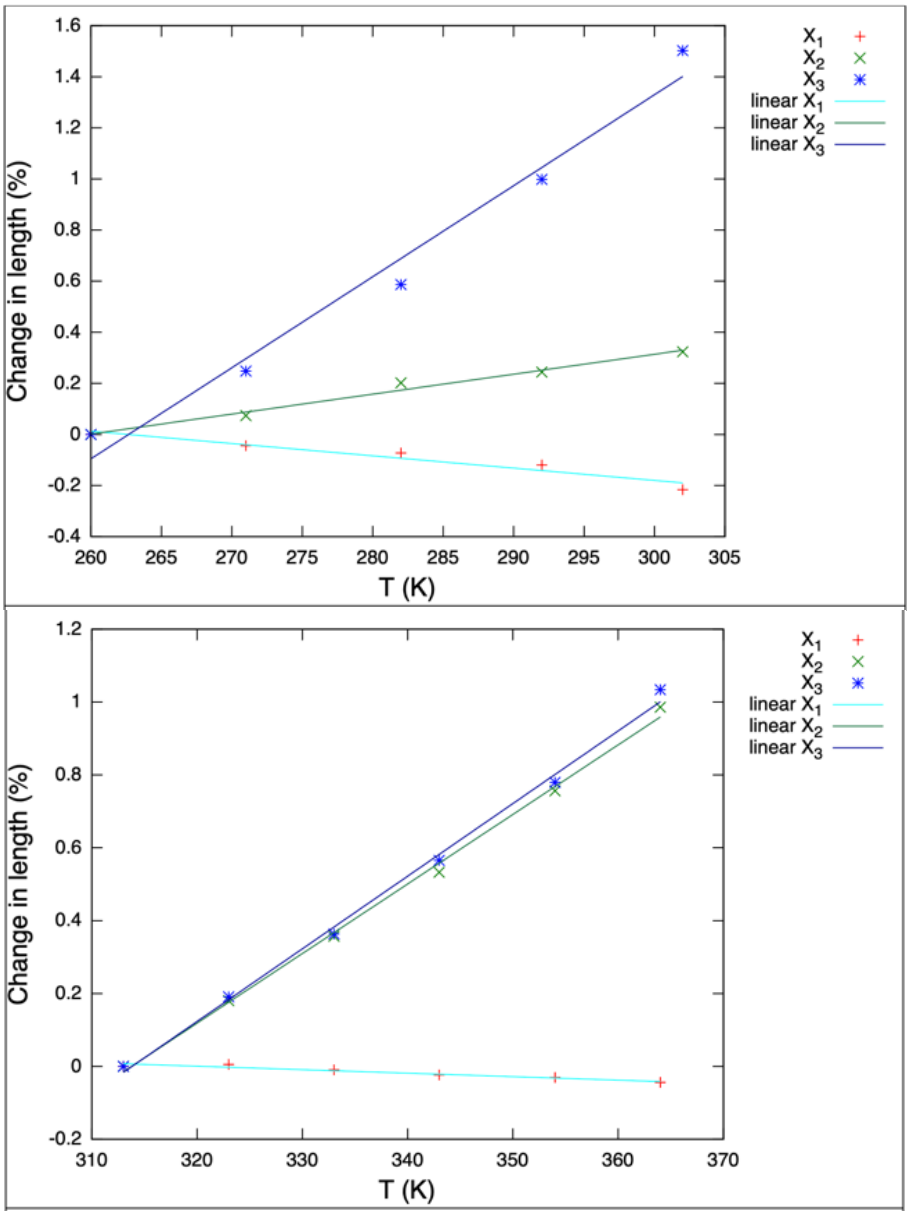

Fig. S8. Changes in lengths of the principal orthogonal axis of phase **III** and **II** as a function of temperature (experimental data are shown in Figure 6). Continuous lines show the linear fitting for the calculation of the thermal expansion coefficients obtained using the PASCal program.

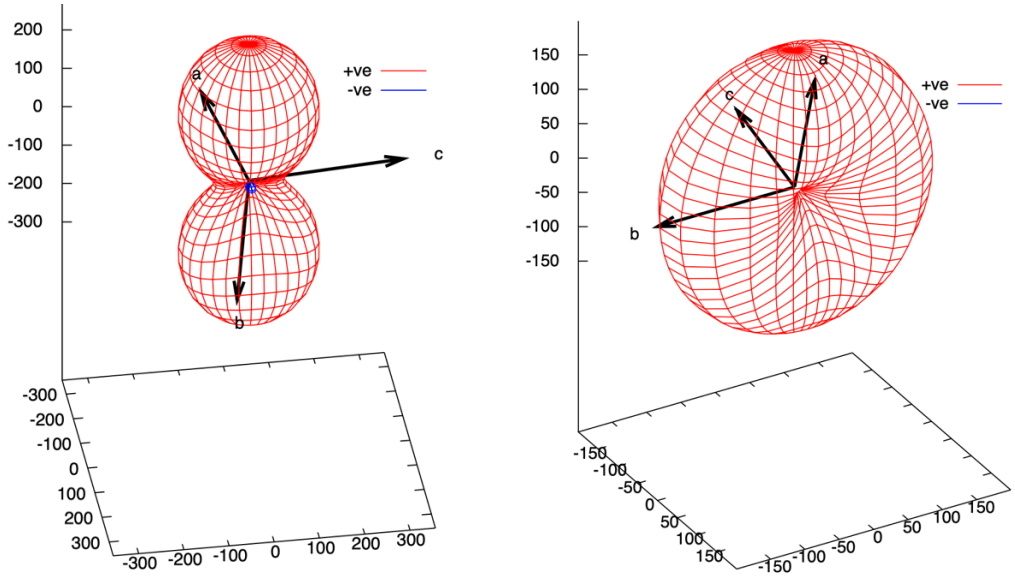

Fig. S9. The thermal expansion indicatrices (red positive; blue negative) of Phase **III** (left) and **II** (right) related to the crystallographic axes (black).

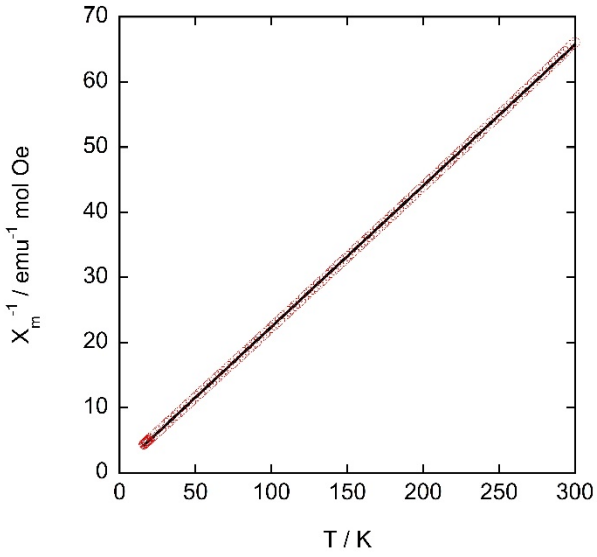

Fig. S10. Fit to the Curie-Weiss law (solid black line) to the magnetic susceptibility data at 1 kOe.

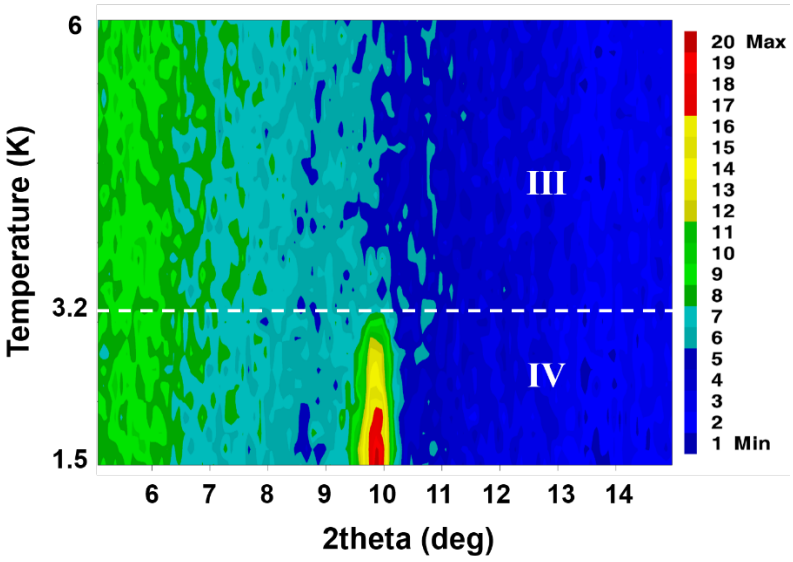

Fig.S11. NPD thermodiffractogram of ((R)-(−)-3-hydroxyquinuclidium)[$FeCl_4$] acquired at D1B from 1.5 to 6 K. The temperature of the disappearance of the magnetic peak is indicated with a dashed white line.

Table S1: Crystallographic data and single-crystal refinement details of ((R)-(−)-3-hydroxyquinuclidium)[$FeCl_4$] at 300 and 100 K from the refinement of the X-ray single-crystal data.

	Phase III @ 150 K	**Phase II @ 300 K**
Empirical formula	$C_7NOH_{14}FeCl_4$	$C_7NOH_{13}FeCl_4$
Formula weight	325.84	324.83
Crystal system	triclinic	monoclinic
Space group	*P*1	*C*2
a (Å)	6.4375(16)	9.257(3)
b (Å)	6.7708(16)	9.852(3)
c (Å)	7.3462(19)	7.466(3)
α (°)	90.147(7)	-
β (°)	91.589(7)	90.704(9)
γ (°)	92.021(7)	-
V (Å^3)	319.87(14)	680.8(4)
Z	1	2
ρ (g·cm^{-3})	1.692	1.585
Reflections [I>2σ(I)]	2473	849
Reflections [all data]	2563	1177
parameters	128	41
Goodness of fit (S)[a]	1.206	1.184
R_1[b]/wR_2[c] [I>2σ(I)]	0.0545/0.1489	0.0946/0.3008
R_1[b]/wR_2[c] [all data]	0.0560/0.1497	0.1140/0.3203

[a] $S = [\sum w(F_0^2 - F_c^2)^2 / (N_{obs} - N_{param})]^{1/2}$. [b] $R_1 = \sum||F_0|-|F_c|| / \sum|F_0|$; [c] $wR_2 = [\sum w(F_0^2)^2 - F_c^2)^2 / \sum w(F_0^2)^2]^{1/2}$; $w = 1/[\sigma^2(F_0^2) + (aP)^2 + bP]$ where $P = (\max(F_0^2,0) + 2F_c^2)/3$, being a = 0.0528 and b = 3.3176

Table S2: Relevant distances of ((R)-(−)-3-hydroxyquinuclidium)[$FeCl_4$] at 10 K obtained from the refinement to the D2B data.

(R)-(−)-3-hydroxyquinuclidium	**Length (Å)**	**FeCl4**	**Length (Å)**	**Fe···Fe**	**Length (Å)**
O1-C4	1.41(3)	Fe1-Cl4	2.182(18)	Fe1···Fe1^{I}	6.323(18)
C1-N1	1.515(19)	Fe1-Cl1	2.183(19)	Fe1···Fe1^{II}	6.797(17)
C1-C2	1.552(19)	Fe1-Cl3	2.194(17)	Fe1···Fe1^{III}	7.24(2)
C2-C3	1.553(19)	Fe1-Cl2	2.210(19)		
C3-C7	1.50(2)				
C3-C4	1.584(19)				
C4-C5	1.564(18)				
C6-N1	1.497(19)				
C6-C7	1.584(19)				
Possible H-bonds:					
X-H···Cl[a]	**Length (Å)**	**Angle (°)**	**a**		
O1-H1···Cl1	2.58(4)	150(3)	*x*, *y*, -1+*z*		
O1-H1···Cl2	2.72(4)	116(3)	*x, y, z*		
N1-H1N···Cl3	2.82(3)	131.9(16)	1+*x, y, z*		
N1-H1N···Cl2	2.88(2)	129.5(16)	1+*x, y, z*		
C1-H1A···Cl2	2.80(3)	162.6(18)	1+*x,* -1+*y, z*		
C1-H1A···Cl1	2.92(3)	115.2(16)	1+*x,* -1+*y,* -1+*z*		
C1-H1AB···Cl3	2.87(3)	144.1(19)	1+*x, y,* -1+*z*		
C5-H5A···Cl2	2.92(3)	113.8(19)	1+*x, y, z*		
C5-H5A···Cl4	2.95(3)	157(2)	*x, y, z*		
C5-H5AB···Cl1	2.83(3)	155(2)	1+*x, y,* -1+*z*		
C6-H6A···Cl2	2.84(3)	148.3(19)	1+*x,* -1+*y, z*		

I: 1+*x*, *y*, *z*; II: *x*, 1+*y*, *z*; III: *x, y*, 1+*z*.

Table S3: Relevant distances of ((R)-(−)-3-hydroxyquinuclidium)[$FeCl_4$] at 150 K obtained from single-crystal X-Ray data.

(R)-(−)-3-hydroxyquinuclidium	**Length (Å)**	**FeCl4**	**Length (Å)**	**Fe···Fe**	**Length (Å)**
C4-O1	1.384(17)	Fe1-Cl4	2.192(3)	Fe1···Fe1^{I}	6.438(2)
C1-N1	1.50(2)	Fe1-Cl2	2.202(3)	Fe1···Fe1^{II}	6.771(2)
C1-C2	1.52(2)	Fe1-Cl1	2.204(3)	Fe1···Fe1^{III}	7.346(3)
C2-C3	1.52(3)	Fe1-Cl3	2.211(4)		
C3-C7	1.50(3)				
C3-C4	1.532(19)				
C4-C5	1.51(2)				
C5-N1	1.50(2)				
C6-C7	1.50(3)				
C6-N1	1.50(2)				

I: 1+*x*, *y*, *z*; II: *x*, 1+*y*, *z*; III: *x*, *y*, 1+*z*.

Table S4: Relevant distances of ((R)-(−)-3-hydroxyquinuclidium)[$FeCl_4$] at RT obtained from single-crystal X-Ray data.

(R)-(−)-3-hydroxyquinuclidium	**Length (Å)**	**FeCl4**	**Length (Å)**	**Fe···Fe**	**Length (Å)**
C2-C3	1.46(8)	Fe1-Cl1	2.19(10)	Fe1···Fe1^{II}	6.759(7)
C2-N1|C1	1.46(9)	Fe1-Cl2	2.19(10)	Fe1···Fe1^{III}	7.466(3)
C3-O1	1.41(10)				
C3-N1|C1^{I}	1.47(9)				
C4-N1|C1^{I}	1.47(8)				
C4-C4^{I}	1.49(3)				

I: 1+*x*, *y*, *z*; II: *x*, 1+*y*, *z*; III: *x*, *y*, 1+*z*.

Table S5. The thermal expansion coefficients (α) and the directions of the thermal expansion tensors of phase **II** and **III**. These values were derived from a linear fitting (continuous lines of Fig. S7 of SI) using orthogonal lattice parameter evolution of synchrotron powder X-ray diffraction data.

	Phase **III**	Phase **II**
α X1/MK^{-1}	-48(6)	-10(1)
direction	(0.26, 0.91, 0.30)	(0.21, 0, -0.98)
α X2/MK^{-1}	78(2)	190(4)
direction	(-0,40, -0.25, 0.88)	(0, -1, 0)
α X3/MK^{-1}	356(27)	199(4)
direction	(0.92, -0.3, 0.26)	(-.94, 0, 0.33)
α V/MK^{-1}	392(20)	383(10)